Effects of frozen storage temperature on the elasticity of tendons from a small murine model

K.L. Goh[1,*], Y. Chen[2], S.M. Chou[3], A. Listrat[4], D. Bechet[4], T.J. Wess[5]

[1]*School of Engineering, Monash University, 46150, Selangor Darul Ehsan, Malaysia*

[2]*School of Chemical & Biomedical Engineering, Nanyang Technological University, Singapore 637459*

[3]*School of Mechanical & Aerospace Engineering, Nanyang Technological University, Singapore 639798*

[4]*Institut National de la Recherche Agronomique, 63122 St Genes-Champanelle, France*

[5]*School of Optometry & Vision Sciences, Cardiff University, Cardiff, CF24 4LU, UK*

Correspondence author: goh.kheng.lim@eng.monash.edu.my

Running head: Effects of frozen storage temperature on tendons

Implications: Ultra-low storage temperature alters (1) the long-range order of collagen packing in fibrils, resulting in fibril rupture at higher stresses, (2) the composition of extra-fibrillar matrix, resulting in an increase in the interaction energy between fibrils via collagen-bound proteoglycans. Consequently, the tissue strength, stiffness, and fracture toughness increase.

Source: *Animal*, page 1-5, The Animal Consortium 2010,

doi:10.1017/S1751731110000698

Abstract

The basic mechanism of reinforcement in tendons addresses the transfer of stress, generated by the deforming proteoglycan-rich (**PG**) matrix, to the collagen fibrils. Regulating this mechanism involves the interactions of PGs on the fibril with those in the surrounding matrix and between PGs on adjacent fibrils. This understanding is key to establishing new insights on the biomechanics of tendon in various research domains. However, the experimental designs in many studies often involved long sample preparation time. To minimise biological degradation the tendons are usually stored by freezing. Here, we have investigated the effects of commonly used frozen storage temperatures on the mechanical properties of tendons from the tail of a murine model (C57BL6 mouse). Fresh (unfrozen) and thawed samples, frozen at temperatures of –20 ºC and –80 ºC, respectively, were stretched to rupture. Freezing at –20 ºC revealed no effect on the maximum stress (σ), stiffness (E), the corresponding strain (ε) at σ, and strain energy densities up to ε (u) and from ε until complete rupture (u_p). On the other hand, freezing at –80 ºC led to higher σ, E and u; ε and u_p were unaffected. The results implicate changes in the long-range order of radially-packed collagen molecules in fibrils, resulting in fibril rupture at higher stresses, and changes to the composition of extra-fibrillar matrix, resulting in an increase in the interaction energy between fibrils via collagen-bound PGs.

Introduction

This paper is concerned with the effects of frozen storage temperature on the elasticity of tendons, which are biological examples of fibre reinforced composites comprising highly paralleled collagen fibrils embedded in the hydrated proteoglycan-rich (**PG**) extracellular matrix (**ECM**) (Hukins & Aspden 1985; Figure 1A). The basic mechanism of reinforcement in tendons addresses the transfer of stress generated in the deforming PG-rich matrix, in response to an external load, to the collagen fibrils (Goh *et al.,* 2005). Regulating this mechanism involves the interactions of PGs on the fibrils with those in the surrounding matrix and between adjacent fibrils (Goh *et al.,* 2007). The stress transfer mechanism is fundamental to understanding the biomechanics of load transmission, from muscle to bone by tendons, in many studies. These studies may be found in biomedical science, e.g. addressing the biomarkers of ageing (Derwin & Soslowsky, 1999), injury and repair (Lin *et al*., 2004), and meat science, e.g. investigating the mechanical response in relation to the quality of the attachment of muscle to bone from livestock (Moussa *et al*., 2007; Gondret *et al*., 2009). Unfortunately, experimental designs in these studies often involve long sample preparation time. To minimise biological degradation tendons are stored by freezing, usually at around -20 ^{o}C (Mousa *et al*., 2007; Goh *et al.,* 2008; Gondret *et al*., 2009) or at ultra-low temperatures, e.g. -80 ^{o}C (Giannini *et al.,* 2008), until the day of testing. Although the processes that regulate the formation of ice crystallites and the disruption of cells and ECM organisation are well-known (Muldrew & McGann, 1990), how frozen storage temperature affects the basic mechanisms that regulate the ECM elasticity, leading to changes in the mechanical properties, is not clear.

We have investigated the influence of frozen storage temperatures on the mechanical properties of tendons from the tail of a small murine model (C57BL6 mouse). Here we are concerned with the maximum stress, σ, on the stress-strain curve, stiffness (E), strain (ε) at σ, strain energy densities up to ε (u) and from ε until complete rupture (u_p) (Goh *et al.,* 2005). Since the genome of the C57BL6 mouse has been sequenced, it has been regarded as an ideal murine model in the context of integrative biology study; it is widely used for laboratory experiments to illuminate basic mechanisms which could address similar outcomes in other mammals (Laissue *et al.,* 2009). In particular, tissues from the murine model have been used extensively to evaluate biomechanical properties to study systemic changes caused by injury and during healing (Lin *et al.,* 2004), ageing of ECM (Goh *et al.,* 2008) and disruption of the signal pathway for regulating ECM in genetically engineered mice that produced alterations in collagen (Derwin & Soslowsky, 1999) and PGs (Derwin & Soslowsky, 1999). Application of the principles of fibre reinforced composites to connective tissues such as tendons has yielded insights on the mechanisms of elastic and plastic stress transfer in collagen fibrils and on fibril-fibril interactions across the hydrated PG-rich matrix within ECM for regulating tissue elasticity (Goh *et al.,* 2005). Here, these insights will be used to speculate on the sensitivity of these mechanisms to low storage temperatures.

Material and Methods

Sample preparation

Tendons, of about 200 microns thick, were dissected from the tail of a 16 month-old mouse (C57BL6) which was sacrificed in accordance with the procedure laid down by

85 the National Research Council for the care and use of laboratory animals. The tendons
86 were transected and divided equally into three groups consisting of ten samples per
87 group. One group was designated as control and was tested immediately. Samples from
88 the second (**M20**) and third (**M80**) groups were immediately placed in freezers operating
89 at -20 ^{o}C (MDF-U5411, Sanyo) and -80 ^{o}C (MDF-U73V, Sanyo), respectively. After 24
90 hours the frozen samples were thawed at room temperature for analysis.

91 *Mechanical tests*

92 A small-scale horizontal tensile rig, designed and built in-house, was used for mechanical
93 tests (Goh *et al*., 2008). Each sample was mounted onto the rig, secured by the grips at its
94 ends and hydrated by submerging in phosphate buffer saline, pH 7.2, at room
95 temperature. The rig was mounted onto an inverted microscope (DM-IL, Leica) for
96 sample observation during the test. A displacement rate of 0.067 mm/s was applied to
97 stretch the sample until the tissue ruptured (Goh *et al*., 2008). The force generated in the
98 sample was recorded by a load-cell (UF-1, Pioden Controls Ltd) coupled to one grip; the
99 sample extension corresponded to the relative displacement of the grips, which was
100 recorded by a linear variable displacement transducer (CDP-M, Tokyo Sokki Kenkyujo).

101 *Determination of mechanical properties*

102 Stress-strain plots were obtained from the load-extension data. Here, stress is defined as
103 the ratio of the load to the nominal cross-sectional area of the sample; strain is the ratio of
104 the change in the sample length to the length described by the grip-to-grip distance. By
105 fitting an appropriate polynomial equation to the data points on the plot, from stress = 0

106 to σ, the point of inflexion was identified (Figure 1B). The gradient at this point
107 parameterised *E* (Goh *et al*., 2008).

108 From the area under the stress-strain curve (Figure 1B), the strain energy density (*u*) up to
109 σ was evaluated to determine the energy needed to cause tissue failure; in this region the
110 energy absorbed is dominated by fibril recruitment and fibril yielding (Goh *et al*., 2008).
111 We have also determined the strain energy density u_p, from ε until when the tissue
112 ruptured completely, to account for the energy absorbed by the dominant failure modes,
113 namely fibril pull-out by frictional sliding at the fibril-PG matrix interface, as well as PG
114 matrix rupture (Sikoryn & Hukins, 1988).

115 *Statistical analyses*

116 Representative (mean ± standard error (**s.e.**)) values of the mechanical parameters, i.e. σ,
117 *E*, ε, ε_y, and *u*, for each treatment were determined. Paired sample t-test was used to
118 analyse for differences between the control versus each treatment group at $\alpha = 0.05$.
119 Differences due to the treatment were considered significant if the P value was less than
120 0.05.

121 **Results**

122 Figure 2 shows stress-strain plots derived from the control, M20 and M80 groups. In
123 general, during the loading stage, all samples featured a toe region followed by a rapid
124 increase in the rate of change of stress with respect to strain; during tissue failure, i.e.
125 beyond the strain at maximum stress, the gradients decreased rapidly until rupture. Of the

three groups, the M80 group yielded the largest gradient during the loading stage and during tissue failure.

Examination of the micro-structure of tendons from the control, M20 and M80 groups revealed wavy collagen fibres (which are one hierarchy above collagen fibrils) which exhibited the usual structural changes, i.e. de-crimping and straightening (Figure 3a), during loading. All the three groups responded with similar structural changes during mechanical loading. Immediately after σ, the tendon began to fail (Figure 3b). Here, a thin section bridging the bulk of tissue was observed (Arrow A). Rupture and pull-out of collagen fibres were also observed; the ends of these structures are indicated by arrow B. At the lower hierarchical level, this could implicate collagen fibril rupture and pull-out. Longitudinal splits in the tendon were also observed, implicating the rupture of the PG matrix (arrow C).

The results of σ, E, ε, u_p and u for the control, M20 and M80 groups are listed in Table 1. In all the cases considered here, no significant difference was observed between the control and M20 groups. No significant difference was observed between the control and M80 groups for ε and u_p. However, the M80 group yielded magnitudes of σ, E and u, which were 1.4, 1.5 and 1.6 times significantly higher, respectively, than the control group.

Discussion

Collagen fibrils feature a crystalline arrangement of collagen molecules. This crystalline arrangement is characterised by a long-range order of radially-packed (side-to-side) collagen molecules and an ordered array of axially staggered collagen molecules along

148 the fibril axis (Laing *et al.,* 2003). The long-range order characterises the crystalline
149 system in which portions deep within the fibril, i.e. far from the fibril-PG matrix
150 interface, exhibit similar strain response; strain energy will not concentrate at the
151 interface but will eventually be absorbed by molecules at greater depths from the
152 interface. Decorin PGs associated with the collagen fibrils consist of a core protein,
153 bound to collagen, with a side chain known as glycosaminoglycans (**GAGs**; Figure 1;
154 Screen *et al,*. 2006). The non-steric interactions between GAGs, from the respective
155 decorin PGs on adjacent fibrils, is implicated for regulating the stress transfer to collagen
156 fibrils as the fibrils slide relative to one another when the tissue is loaded (Screen *et al.,*
157 2006; Goh *et al.,* 2007). According to the elasticity of materials (Sun, 2009), it follows
158 that E and σ may be determined by equilibrating the external mechanical load to the
159 responses of the inter-molecular forces of the tendons. Thus,

$$E \propto U_1 / V \,, \tag{1}$$

$$\sigma \propto U_2 / V \,, \tag{2}$$

160 where U_1 and U_2 are the sum of cohesive energy per bond, at equilibrium between the
161 biomacromolecules, within a volume, V (Sun, 2009). Although E and σ have similar
162 dimensions, the molecular interactions involved in these parameters are not the same.
163 Equation (1) is valid whether the tendon is undergoing elastic or plastic deformation,
164 which is determined by the forces of interactions between the GAGs of decorin PGs on
165 adjacent collagen fibrils. Equation (2) is only valid when the tendon is experiencing
166 plasticity, which could involve the plastic deformation of fibrils and the breaking of
167 covalent bonds between collagen molecules in the fibril. Thereafter, the broken bonds

could inhibit the motion of collagen molecules around the dislocations, leading to a strengthened tissue as energy of the remaining bonds increases and the bond length contracts (Sun, 2009).

It follows that any increase in E is regulated by the Van Der Waals (**VDW**) forces between GAGs from collagen-bound PGs, at adjacent fibrils. The interactions are significant for as long as the fibrils are in close proximity to one another. During freezing, as water withdraws from the water compartment, beginning in the PG matrix (Bevilacquar *et al*., 1979), and precipitates into ice crystallites, the ion concentration increases in the non-water compartment (Muldrew & McGann, 1990), creating a concentration gradient across the unfrozen zone. As cations (e.g. Na^+) diffuse to the anionic charge of the GAGs, the increase in the concentration of cations around the GAGs increases the attractive forces between the GAGs. This effect may be appreciable at -80 ^oC but not at -20 ^oC. Moreover, the changes occurring in the tendons from the M80 group may not be completely reversible during thawing; in this case, a greater GAG-GAG interaction increases the resistance for fibril-fibril sliding when the tissue is stretched so that the tissue becomes stiffer than unfrozen ones. To understand how this could have happened, a molecular model was developed to study GAG-GAG interactions (following from Redaelli *et al.,* 2003). Mobile cations, namely Na^+, were designated in closed proximity to each group to model a hypertonic PG matrix environment; the number of Na^+ (N) was varied to investigate the effects on the VDW energy which was evaluated as a function of the distance between the PG molecules, δ. The model was solved by molecular mechanics using software Hyperchem (Version 7.5, Hypercube, Inc.). It was found that VDW energy, which decreased as δ increased, was affected by N.

191 In particular, VDW energy increased by about 1.2 times as *N* increased two-fold but the
192 profile of the energy-δ curves was not affected. Further details can be found in
193 supplementary material. Thus we concluded that the overall effect of freezing led to a
194 localisation and densification of charge and energy. Hence *E* has to increase as predicted
195 by Equation (1).

196 Any increase in σ could be attributed to changes in the packing of collagen molecules in
197 the fibril. Low storage temperature could alter the long-range order of radial packing of
198 collagen molecules, which could be assessed by the diffuse scatter region from x-ray
199 diffraction patterns of these tissues. Changes to the diffuse region occur during freezing;
200 tissues frozen at -150 ºC exhibit reduced diffuse regions suggesting that the long range
201 order is increased (Laing *et al*., 2003). Whether the effect is reversible upon thawing is
202 not clear; Hickey and Hukins (1979) had shown that thawed tissues (frozen at -35 ºC)
203 exhibited smaller diffuse regions as compared to control samples. An increase in the
204 long-range order implies that the fine structure, i.e. the crystalline arrangement of
205 collagen molecules, of the fibril would have to be disturbed to a very much greater depth.
206 More molecules would be involved in absorbing the energy needed to cause fibril
207 rupture; thus more energy is absorbed by the tissue. As pointed out earlier in this section,
208 stresses will not concentrate at regions near to the fibril surface, an important factor
209 determining the failure of fibrils. Instead, stresses will be distributed deeper within the
210 fibril, thus making the fibril less susceptible to fracture so that a higher *u*, and
211 consequently higher σ as predicted by Equation (2), would be needed to rupture the
212 tendon.

We note that u_p is not affected by low storage temperatures. This suggests that low storage temperature did not have a significant effect on the molecular interaction at the fibril-PG interface and in the bulk of the PG matrix. We also note that the extensibility of the tendon, which is parameterised by ε, was not sensitive to low storage temperatures. We recalled that x-ray diffraction patterns of stretched tendons revealed that the tissue strain would always be larger than the strain within the collagen fibrils (Puxkandl *et al.*, 2002). It is possible that the changes affecting the strain in individual fibrils would have negligible influence on the overall strain at maximum stress in the tissue stored at sub-zero temperature.

The purpose of this paragraph is to discuss the effects of cooling on the size of the ice crystallites formed in the tendons. According to Bevilacqua *et al*. (1979), a combination of the effects of solute concentration (due to an increase in viscosity) and thermal gradients (due to latent heat release and heat lost from the unfrozen zone), in the region between the crystallites, could lead to super-saturation and super-cooling. Theoretically, the cooling rate of the tissue is proportional to the square of the moving speed of the freezing front, u^2, while the temperature gradient at the solid-liquid interface (G) is proportional to u (Miyawaki *et al*., 1992). Here, $G = [T_m - T_s]/x$ where x is the length of the frozen crystallite and T_s and T_m are the operating temperature of the freezer and the temperature at the surface of the crystallite, respectively. Empirically, the thickness (d_p) of ice crystallites is related to u and G; this relationship can be represented as

$$d_p \propto 1/\sqrt{uG} \tag{3}$$

(Tiller & Rutter, 1956). It follows that the cooling rate is related to d_p in Equation (3). Thus, slow freezing rates cause ice to grow in extracellular locations, resulting in large crystallites and maximum dislocation of water; rapid cooling produces small ice crystallites in both cells and extracellular matrix (Bevilacqua *et al*., 1979). In particular, slow cooling rates correspond to wider spread of sizes; fast cooling rates correspond to narrower spread of sizes and the crystallite growth is more organised (Pardo *et al*., 2002). Consider a model of the crystallite in the tendon. Based on the results of Bevilacqua *et al*. (1979) and Chevalier *et al*. (2000), using an order of magnitude estimate, we find $x \sim 100$ μm. Owing to convection in the freezers, we may approximate $T_s \sim T_f$, = 0 ºC, the freezing temperature of water. With these values, Eq. (3) was evaluated for the upper limit (0.41 mm/s; Miwayaki *et al*., 1992) and lower limit (0.06 mm/s; Chevalier *et al*., 2000) of u, i.e. corresponding to four combinations, for each case of T_m = -20 ºC and -80 ºC. By determining the ratio $d_p|_{-20^\circ C} / d_p|_{-80^\circ C}$, this simple analysis predicts that the ice crystallites formed at the higher freezer temperature are bigger that those formed at the lower freezer temperature by 1.16 to 3.46 times. In this case, the more organised smaller crystallites are dispersed uniformly within the inter-fibrillar matrix, raising the ion concentration around the GAGs. This argument complements an earlier suggestion that the increase in GAG interactions, arising from a localisation and densification of charge and energy around the GAGs associated with collagen fibrils, yields a higher E.

In conclusion, ultra-low storage temperature affects only σ, E and u in tail tendons from the C57BL6 mouse, leading to tissues with larger σ, E and u. The results of this study imply that care is required when considering the method for storing and preserving tendons in order to minimise changes to the elasticity of the tissue.

256 **Acknowledgements**

257 CY was supported by an NTU research scholarship. This work was supported by grants
258 from the EU Framework V, and the Merlion-France 2007 program (from the French
259 Ministere des Affaires Etrangeres et Europeennes).

260 **References**

261 Bevilacqua A; Zaritzky N and Calvelo A 1979. Histological measurements of ice in
262 frozen beef. *Journal of Food Technology* 14, 237-251.

263 Chevalier D, Le Bail A, Ghoul M 2000. Freezing and ice crystals formed in a cylindrical
264 food model: part I. Freezing at atmospheric pressure. *Journal of Food Engineering* 46,
265 277-285.

266 Derwin KA and Soslowsky LJ 1999. A quantitative investigation of structure function
267 relationships in a tendon fascicle model. *Journal of Biomechanical Engineering –*
268 *Transactions of the ASME*,121, 598-604.

269 Giannini S, Buda R, Di Caprio F, Agati P, Bigi A, De Pasquale V and Ruggeri A 2008.
270 Effects of freezing on the biomechanical and structural properties of human posterior
271 tibial tendons. *International Orthopaedics* 32, 145-151.

272 Goh KL, Meakin JR, Aspden RM and Hukins DWL 2005. Influence of fibril taper on the
273 function of collagen to reinforce the extra-cellular matrix. *Proceedings of the Royal*
274 *Society of London* B272, 1979-1983.

275 Goh KL, Meakin JR, Aspden RM and Hukins DWL 2007 Stress transfer in collagen
276 fibrils reinforcing connective tissues: Effects of collagen fibril slenderness and relative
277 stiffness. *Journal of Theoretical Biology* 245, 305-311.

278 Goh KL, Holmes DF, Lu H-Y, Richardson S, Kadler KE, Purslow PP and Wess TJ 2008.
279 Ageing changes in the tensile properties of tendons: influence of collagen fibril volume
280 fraction. *Journal of Biomechanical Engineering - Transactions of the ASME* 130
281 (021011).

282 Gondret F, Hernandez P, Remignon H and Combes S 2009. Skeletal muscle adaptations
283 and biomechanical properties of tendons in response to jump exercise in rabbits. *Journal*
284 *of Animal Science* 87, 544-553.

285 Hickey DS and Hukins DWL 1979. Effect of methods of preservation on the arrangement
286 of collagen fibrils in connective tissue matrices: an x-ray diffraction study of annulus
287 fibrosus. *Connective Tissue Research* 6, 223-228.

288 Hukins DWL and Aspden RM 1985. Composition and properties of connective tissues.
289 *Trends in Biochemical Sciences* 10, 280-284.

290 Laing J, Cameron GC and Wess TJ 2003. Molecular organisation of collagen fibrillar
291 structures – A review. *Recent Research Developments in Molecular Biology* 1, 51-71.

292 Laissue P, L'Hote D, Serres C and Vaiman D 2009. Mouse models for identifying genes
293 modulating fertility parameters. *Animal* 3, 55-71.

294 Lin TW, Cardenas L and Soslowsky LJ 2004. Biomechanics of tendon injury and repair.
295 *Journal of Biomechanics* 37, 865-877.

296 Miwayaki O, Abe T and Yano T 1992. Freezing and ice structure formed in protein gels.
297 *Bioscience and Biotechnology in Biochemistry* 57, 953-957.

298 Moussa M, Babile R, Fernandez X and Remignon H 2007. Biochemical and
299 biomechanical properties of tendons in two commercial types of chickens. *Animal* 1,
300 983–988.

301 Muldrew K and McGann LE 1990. Mechanisms of intracellular ice formation.
302 *Biophysical Journal* 57, 525-532.

303 Pardo JM, Suess F and Niranjan K 2002. An investigation into the relationship between
304 freezing rate and mean ice crystal size for coffee extracts. *Transactions of IChemE* 80,
305 176-182.

306 Puxkandl R, Zizak I, Paris O, Keckes J, Tesch W, Bernstorff S, Purslow P and P Fratzl P
307 2002. Viscoelastic properties of collagen: synchrotron radiation investigations and
308 structural model. *Philosophical Transactions of the Royal Society London B* 357, 191–
309 197.

310 Redaelli A, Vesentini S, Soncini M, Vena P, Mantero S and Montevecchi FM 2003. The
311 possible role of decorin glycosaminoglycans in fibril to fibril force transfer in relative
312 mature tendons—a computational study from molecular to microstructural level. *Journal*
313 *of Biomechanics* 36, 1555–1569.

314 Screen HRC, Chhaya VH, Greenwald SE and Bader DL 2006. The influence of swelling
315 and matrix degradation on the microstructural integrity of tendon. *Acta Biomaterialia* 2,
316 505-513.

317 Sikoryn TA and Hukins DWL 1988. Failure of the longitundinal ligaments of the spine.
318 *Journal of Materials Science Letters* 7, 1345-1349.

319 Sun CQ 2009. Thermo-mechanical behavior of low-dimensional systems: The local bond
320 average approach. *Progress in Materials Science* 54, 179-309.

321 Tiller WA and Rutter JW 1956. The effect of growth conditions upon the solidification of
322 a binary allow. *Canadian Journal of Physics* 34, 96-121.

323 **Figure Legends**

324 Figure 1 (A) Extracellular matrix of tendons comprising of collagen fibrils embedded in a
325 hydrated proteoglycan-rich matrix. Decorin core proteins, with glycosaminoglycans
326 (GAGs) attached, are depicted on the surface of collagen fibrils. (B) A stress-strain curve
327 (M20) illustrating the areas under the curve corresponding to the strain energy density to
328 maximum stress (u) and to fracture (u_p); arrows P1 and P2 indicate the point of inflexion
329 and the maximum stress (σ), point respectively.

330 Figure 2. Plot of stress versus strain from control and treated samples. Data points
331 represent a typical experiment from one sample each.

332 Figure 3. Microscopic examination of tendon samples (a) during initial loading, (b) post-
333 peak stress, σ. The images in part a and b were taken from a sample belonging to the
334 M20 (samples treated at -20 ^{o}C) group. Horizontal (scale) bar has a length of 100 μm.
335 Arrow A indicates a thin section bridging the bulk of tissue. Arrow B indicates the ends
336 of the fibres. Arrow C indicates longitudinal splits in the tendon.

337

Tables

Table 1. *Mechanical properties of tail tendons from the C57BL6 mouse*

	σ (MPa)	*E* (MPa)	*u* (MPa)	u_p (MPa)	ε
Control	55.0 ± 4.9	434.2 ± 39.5	6.1 ± 0.7	2.5 ± 0.9	0.199 ± 0.008
M20	59.0 ± 3.4	534.0 ± 28.3	6.3 ± 0.5	1.8 ± 0.2	0.184 ± 0.005
M80	79.5 ± 9.7 *	644.5 ± 71.7 *	10.0 ± 1.6 *	1.4 ± 0.2	0.202 ± 0.011

Values are mean ± s.e. (n = 10).

∗Significant difference of treatment (with respect to the control) at $P < 0.05$.

Abbreviations are: M20 = samples treated at -20 ºC; M80 = samples treated at -80 ºC; s.e. = standard error.

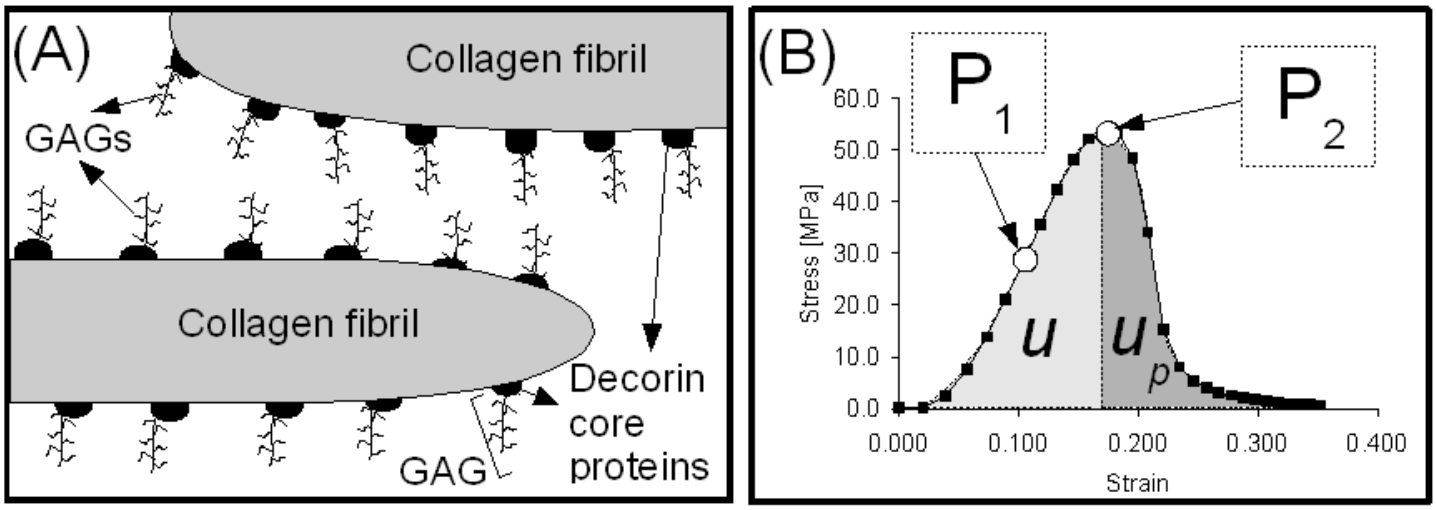
(A)
Collagen fibril
GAGs
Collagen fibril
Decorin
core
proteins
GAG
(B)
P 1
P 2
60.0
50.0
40.0
30.0
20.0
10.0
0.0
Stress [MPa]
u
u p
0.000
0.100
0.200
0.300
0.400
Strain

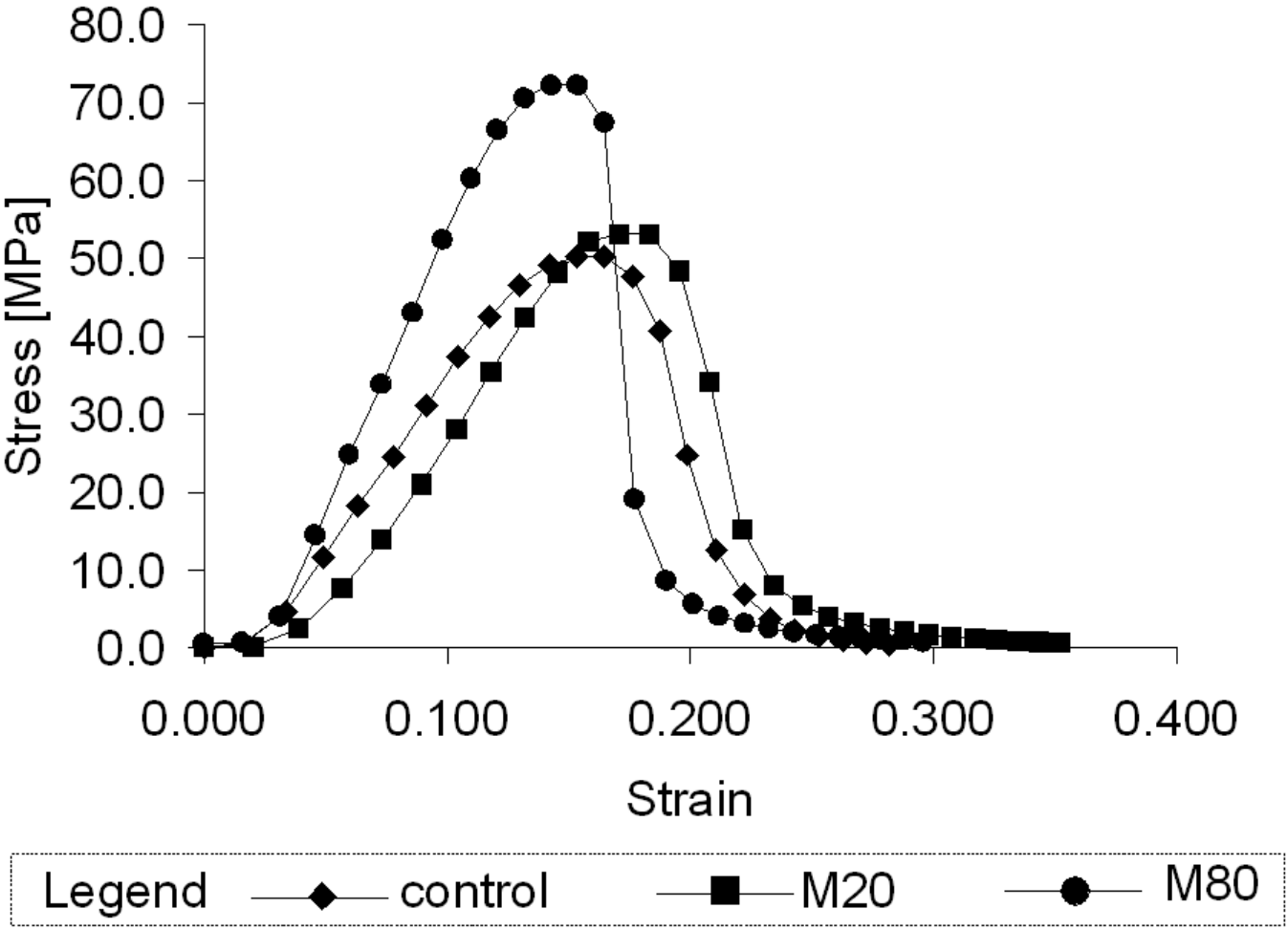
80.0
70.0
60.0
50.0
40.0
30.0
20.0
10.0
0.0
Stress [MPa]
0.000
0.100
0.200
0.300
0.400
Strain
Legend
control
M20
M80

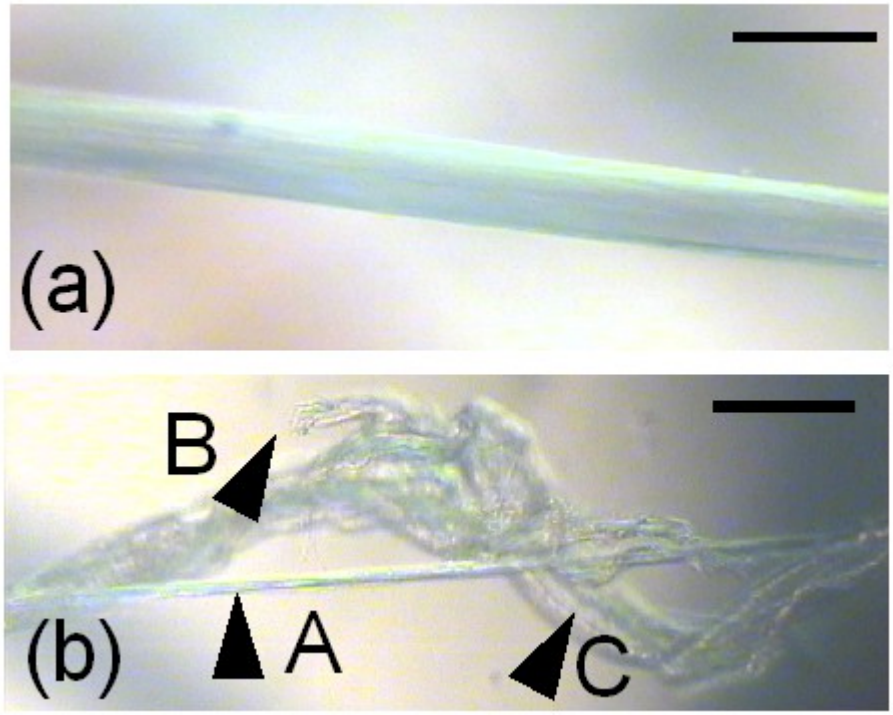
(a)
B
(b)
A
C

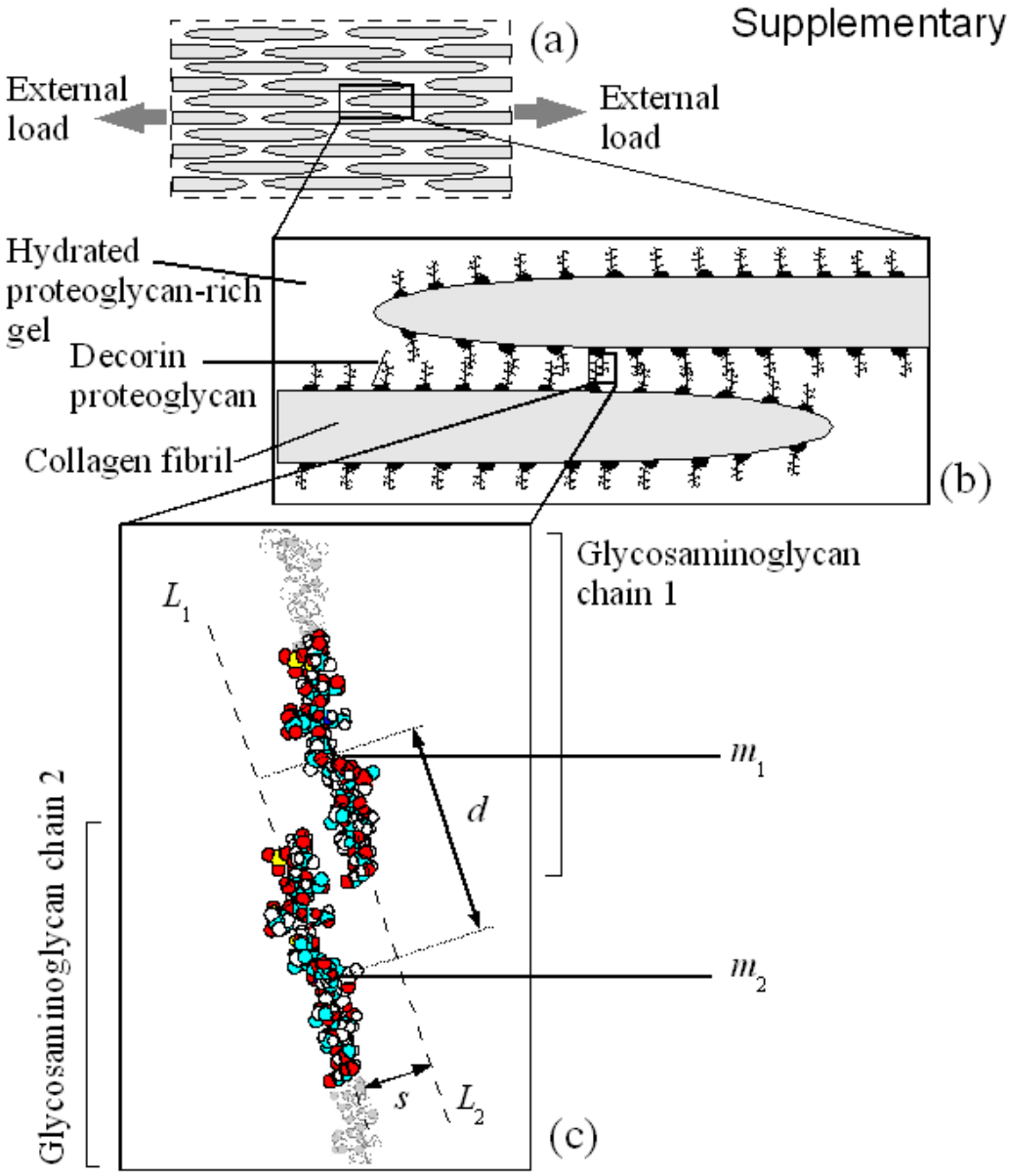

Figure 1S Molecular mechanics study of decorin interactions on adjacent fibrils. A model was developed to evaluate the relationship between VDW energy and cation number density (ρ) under fibril-fibril sliding action (a-b). As shown in (c), the model displays the GAG chains (comprising chondroitin-4-sulfate disaccharide repeats) associated with decorin molecules on adjacent fibrils in close proximity. Here, *s* and *d* denote the separation and displacement between m_1 and m_2 which are the mid-points within the last four repeats of each GAG chain. L_1 and L_2 are the labels for the axes (long dashes) corresponding to GAG chain 1 and 2, respectively.

Supplementary material

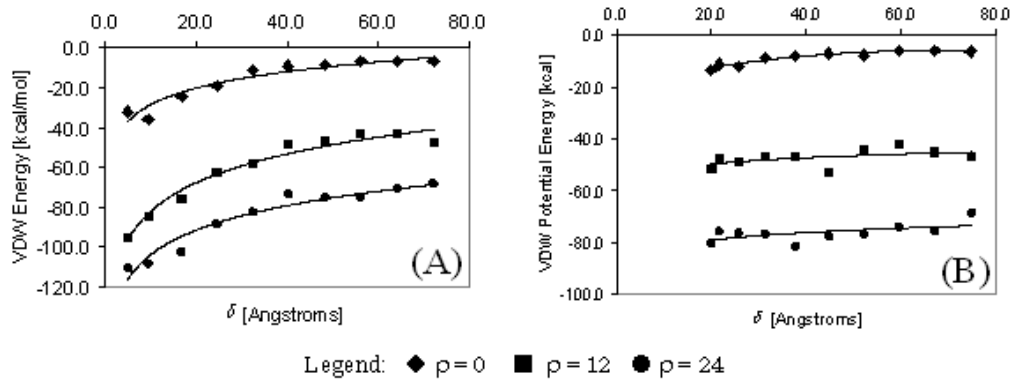

Figure 2S. Graphs of Van Der Waals (VDW) potential energy versus sliding distance δ for (A) s = 5 Å and (B) s = 20 Å. Here, VDW energy was evaluated from the model (see Figure 1S) as a function of δ, where $\delta^2 = s^2 + d^2$. An initial condition was used to describe the GAG-GAG overlapping distance over four chondroitin-4-sulfate disaccharide repeats. Each disaccharide repeat is negatively charged due to the anionic nature of the sulphate and carboxylate groups. Restraints on each chain were implemented to maintain the semi-rigid linear conformation of the chain. Solvent environment was modelled implicitly; the dielectric constant was assigned a value of 80 to correspond to water. The model was implemented using software Hyperchem (Version 7.5, Hypercube, Inc.). Geometry optimisation was investigated using molecular mechanics (AMBER3 force field); the Polak Ribiere (conjugate gradient) algorithm was used to determine the minimum energy value. Atomic partial charges were evaluated successively on the sulphate group and carboxyl group, where the total charge value = -1 for each group, using the single point calculation. Mobile cations (Na^+) were designated in closed proximity to each group to model a hypertonic PG matrix environment.The model predicted that VDW energy increases by about 1.2 times as the number of cations increases two-fold. The value of ρ also influences the rate of decrease in VDW energy with respect to δ between the GAGs. The predictions show that VDW energy decreases least rapidly as δ increases when ρ = 24. However, VDW energy decreases most rapidly for ρ = 0.